Selective electrochemical reactivity of rutile VO_{2} towards the suppression of metal-insulator transition

Sujay Singh, Tesfaye A. Abtew, Gregory Horrocks, Colin Kilcoyne, Peter M. Marley, Adam A. Stabile, Sarbajit Banerjee, Peihong Zhang, and G. Sambandamurthy

Phys. Rev. B **93**, 125132 — Published 21 March 2016

DOI: 10.1103/PhysRevB.93.125132

Selective Electrochemical Reactivity Of Rutile VO_2 Towards The Suppression of Metal-Insulator Transition

Sujay Singh[1], Tesfaye A. Abtew[1], Gregory Horrocks[2,3], Colin Kilcoyne[1], Peter M Marley[2,3], Adam A. Stabile[1], Sarbajit Banerjee[2,3], Peihong Zhang[1], and G. Sambandamurthy[1]*

[1]*Department of Physics*

[2]*Department of Chemistry, University at Buffalo,*

State University of New York, Buffalo, NY 14260, USA and

[3]*Department of Chemistry, Texas A&M University, College Station, TX 77843, USA*

We demonstrate through electrolyte gating measurements of a single nanobeam that the rultile phase of VO_2 is electrochemically more reactive than the monoclinic phase. Our results show that the complete suppression of the metal to insulator transition and stabilization of the metallic phase is possible when gate voltage is applied in the rutile metallic phase. The results are discussed based on the formation of oxygen vacancies wherein accommodation of a high concentration of vacancies in the rutile phase selectively stabilizes it by disrupting dimerization of adjacent V-V pairs required for transition to the monoclinic phase. The creation of oxygen vacancies is proposed to proceed through the oxidation of the electrolyte. Raman spectroscopy data suggest surface metallization upon electrolyte gating with initial coexistence of insulating monoclinic and metallic domains. The selective electrochemical reactivity of the rutile phase and the resulting defect-induced stabilization of this phase across a vastly expanded temperature window suggest a facile defect engineering route to tune electronic phase transitions.

PACS numbers: 71.30.+h, 73.40.Mr, 71.15.Mb, 78.30.cd, 61.72.jd, 73.20.-r

I. INTRODUCTION

Strongly correlated oxides are extremely sensitive to defects such as oxygen vacancies that can be further engineered to tune the electronic and magnetic properties in these systems[1–5]. VO_2, a widely studied correlated electron material, exhibits a metal to insulator transition $\sim$ 342 K[6] that coincides with a structural phase transition from a monoclinic insulator to a rutile metal. This concurrent appearance of an electronic transition with a structural transition shows how the lattice, orbital and possibly spin degrees of freedom are closely related and provides exciting ways to controllably tune the rich phase diagram of VO_2 by several means. The creation of oxygen vacancies is one such way to engineer defects in oxides to modulate the electronic properties and possibly tune phase transitions. A recent experiment on VO_2 showed modulations in the electronic properties by the introduction of oxygen vacancies via electrolyte gating[7]. Nevertheless, physical interpretations of electrolyte gating induced effects in correlated oxides are hotly debated due to the questions about the cause being electrostatic[8–11] and/or electrochemical[7,12–18] in nature. Recently, the conductance modulation in electrolyte gated VO_2 was controlled by a graphene monolayer at the oxide-liquid interface indicating that the changes to be electrochemical in nature[19].

The creation of oxygen vacancies is known to be dependent on the crystal structure and the surface planes in oxides such as CeO_2 and TiO_2[16,18,20,21]. In VO_2, despite the recent experiments, the differences in the electrochemical reactivity of and the creation of oxygen vacancies in individual structural phases of VO_2 (monoclinic and rutile) and their implications on altering the electronic phase diagram of VO_2 have not been systematically studied. In this work, we show, through electrolyte gating studies of single crystalline VO_2 nanobeams and through *ab initio* calculations, that the electrochemical reactivity of the metallic rutile VO_2 is distinctly different from that of the insulating monoclinic phase. Hence, the full suppression of the metal to insulator transition (MIT) or the stabilization of the metallic phase to lower temperatures is possible only if the gate-induced modulations are initiated in the rutile phase. We discuss our experimental data in light of oxygen vacancies creation during electrolyte gating measurements as previously observed[7,15–18]. Our density functional theory (DFT) results show that the creation of oxygen vacancies in the rutile phase results in disturbing the V-V dimerization that can lead to the stabilization of the rutile phase to lower temperatures. Furthermore, we suggest that the creation of

oxygen vacancies is thermodynamically favorable if the removed oxygen atoms oxidize the bis(trifluoromethylsulfonyl)imide (TFSI) anions present in the most commonly used ionic liquid *N*,*N*-diethyl-*N*-methyl(2-methoxyethyl)ammonium bis(trifluoromethylsulfonyl)imide (DEME-TFSI).

II. EXPERIMENTAL SET UP AND DEVICES

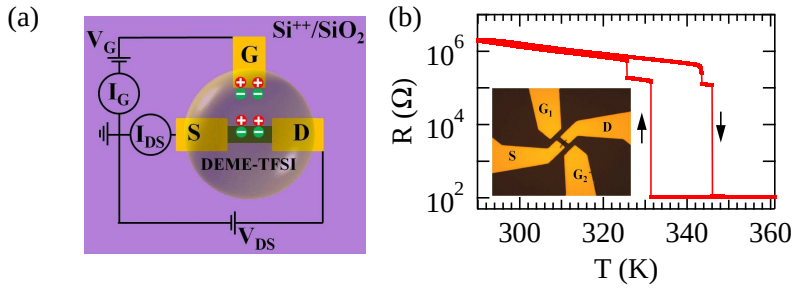

FIG. 1. (a) Schematic of the experimental set up for electrolyte gating of VO_2 nanobeams. (b) Resistance as a function of temperature ($R-T$ plot) at zero gate voltage for a typical device; the arrows indicate the direction of T sweep. The device undergoes a massive insulator-metal transition at $T_C \sim 346$ K. Inset shows the picture of a device.

The VO_2 nanobeams used in the study were grown by a stepwise hydrothermal process and the details about the synthesis and the structural characterization can be found elsewhere[22]. The devices were made of individual nanobeams of single crystalline VO_2 with lengths ranging from 10 to 30 μm and widths from 200 to 800 nm. The nanobeams sprayed on to Si/SiO_2 substrates to yield devices free from any inherent substrate strain. Electrodes (source, drain, and gates) were defined through a standard photolithography process and metal contacts (Cr/Au) were deposited by electron beam evaporation. For the electrolyte gating measurements, a single drop (diameter of 200-300 μm) of the electrolyte (DEME-TFSI) (from Ionic Liquids Technologies) is placed on top of the device such that it covers the electrodes and the nanobeam. Fig. 1 (a) shows the schematic of the experimental set up used for the modulation of the resistance of VO_2 nanobeams by ionic liquid (IL) gating. Inset of Fig. 1 (b) shows a typical device with a 5 μm separation between the source

(S) and the drain (D); the gate electrodes G_1 and G_2 are separated by 25 μm. The gate measurements, both V_G and T sweeps, were performed with a constant drain-source bias (V_{DS}) of 0.05 V. The gate voltage was applied at the gate electrode (G_1 or G_2) and the VO_2 nanobeam was connected to the ground as shown in Fig. 1 (a). The gate leakage current (I_G) and the source-drain current (I_{DS}) were measured independently and all the electrical measurements were performed using Keithley 2400 source meters. The gate voltages (V_G) were applied at 360 K (rutile phase) prior to measuring resistance (R) while varying temperature (T) measurements to maximize the redox kinetics. The device exhibits a massive MIT $\sim$ 346 K accompanied by a more than four orders of magnitude change in resistance (Fig. 1 (b), measured at zero gate voltage). Upon cooling, the device returns to the insulating state at 332 K, with a hysteresis of 14 K.

III. ELECTROLYTE GATING MEASUREMENTS

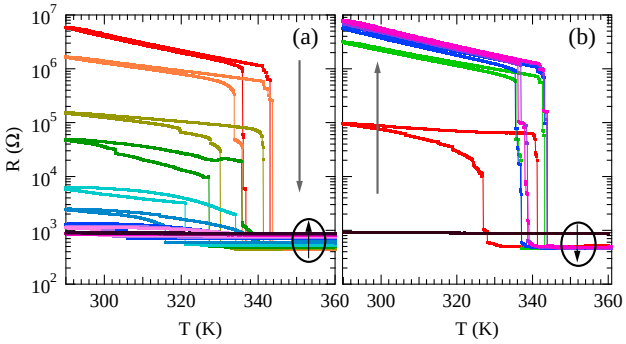

FIG. 2. (a) $R-T$ plots at fixed $+V_G$ values (applied at 360 K) from 0 V (red trace) to 2.2 V (brown trace) in steps of 0.2 V. The MIT is fully suppressed without any hysteresis at $V_G = 2.2$ V. Resistance of the metallic phase increased by $\sim$ 450 Ω at $V_G = 2.2$ V as compared to $V_G = 0$ V suggesting that the gating induced metallic phase is different from a thermally induced one. (b) $R-T$ plots measured at different $-V_G$ values (starting from red trace at zero bias to pink trace at every -0.2 V) show an increase in R with V_G. The device was fully recovered to the initial state at $V_G = -0.8$ V.

Fig. 2 (a) shows $R-T$ plots measured at various positive V_G. The device resistance decreased progressively with the increase in V_G, the MIT was fully suppressed at $V_G = +2.2$

V without any hysteresis. However, the resistance in the metallic phase increased with V_G (440 Ω at $V_G = 0$ V at 360 K and 880 Ω at $V_G = +2.2$ V) suggesting that the ionic liquid (IL) gating induced metallic phase to be different in nature than the thermally induced metallic phase[17].

After the suppression of the MIT, the device was stable in vacuum for days even after ramping back to $V_G = 0$ V however the recovery was faster in air. For example, the device was left in air for 10 hours at $V_G = 2.2$ V at 360 K and the resistance relaxed to 550 Ω indicating a partial recovery of stoichiometry by capturing atmospheric oxygen. The increase of resistance in the metallic phase during gating is consistent with the creation of oxygen vacancies[7,15–18] that appears to have an analogous effect on the electronic phase transition as the introduction of dopants as evidenced by the recovery when exposed to air. The relaxation towards lower resistance in air is a sign of the inclusion of oxygen atoms. After treating the device in air, $R-T$ plots were measured at various negative V_G values to fully restore it to its initial state. R traces in Fig. 2 (b) show an increase with the increase in $-V_G$ and the device was fully recovered at $V_G = -0.8$ V.

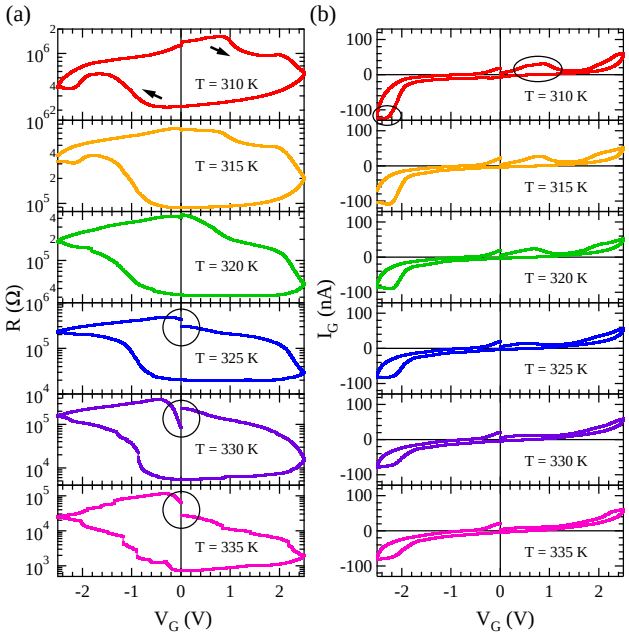

FIG. 3. (a) R vs. V_G and (b) I_G vs. V_G traces from the insulating phase. While reversible changes in R can be seen at T = 310-320 K over the V_G cycle, irreversible changes (circles) set in at higher T. Asymmetric behavior in the values of I_G and in the position and size of the peaks (ovals in (b)) pointing to dissimilar chemical kinetics.

In order to understand the electrochemical reactivity of monoclinic VO_2, gate sweeps measurements were performed at various fixed T in the insulating phase. Fig. 3 (a) shows the modulations in R with V_G in the insulating phase of the nanobeam at various temperatures from 310 K to 335 K (the arrows show the direction of the gate sweep). As V_G increases from 0 to 2.5 V, R decreases. Now, when the V_G is reduced but still positive, R continues to decrease until the polarity of V_G is reversed. The device can be fully restored to its initial state if V_G is then swept to -2.5 V and back to 0 V. However, drifts (marked with circles) from the initial insulating states, leading to irreversible changes, were observed even after the $-V_G$ sweeps at higher temperatures (325 K to 335 K). Assuming oxygen vacancies to be behind the R modulation, it can be inferred for the monoclinic insulating phase that the concentration of oxygen vacancies is not high enough to obtain a metallic phase possibly due to the relatively high formation energy (and/or barriers). However, the resistance clearly drops with increasing V_G and T indicating enhanced conductivity due to oxygen vacancy.

Fig. 3 (b) shows the behavior of the gate leakage current (I_G) as V_G was swept. Several intriguing observations can be made: the presence of peaks (ovals) in the I_G-V_G plots suggests possible redox reaction at the IL/VO_2 interface during the gating process[7,23–26]. It is interesting to note that the I_G-V_G traces look similar to cyclic voltametry (CV) plots for electrochemical measurements that require three electrodes - working, reference and counter electrodes. The characteristics of a CV plot depend on the kinetics of charge transfer between the electrolyte and the electrode, the charge diffusion to the electrolyte/electrode interface, chemical reactions involving electroactive species, and the voltage scan rate[23–25]. In Fig. 3 (b), the peaks at positive and negative gate biases are asymmetric in their positions and sizes. This shows that the redox kinetics at positive and negative biases are different and some of the electroactive species are likely consumed irreversibly during the gating process and resulting in the absence of a peak at negative V_G corresponding to peaks, say at $V_G \sim 0.8$ V. The largest peaks were observed at 310 K, however the gradual decrease in the peak size with increasing T is suggestive of the decrease in reaction rate due to the progressive depletion of reactants at the IL/VO_2 interface due to multiple gate sweeps. Larger peaks were observed in the rutile phase due a temperature effect and will be discussed later in Fig. 4 (b). It should be noted that at positive gate bias, DEME cations will accumulate near VO_2 whereas TFSI will accumulate near VO_2 in case of negative gate bias. The magnitude of I_G at $V_G = -2.5$ V was twice than that at $V_G = +2.5$ V suggesting increased redox activity

when TFSI accumulates at the VO_2 nanobeam that acts as anode at negative gate bias values.

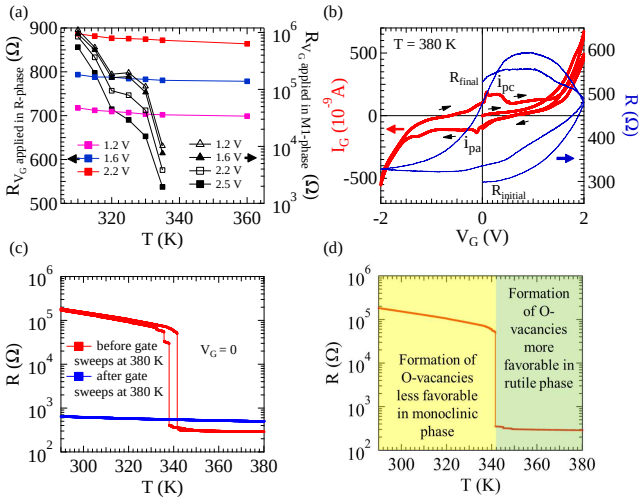

FIG. 4. (a) Comparison of electrochemical reactivity of rutile (R) and monoclinic (M1) phase in the temperature range 310 to 360 K. The left axis shows R modulation when various V_G was applied in R-phase (at 360 K) as compared to the R modulation (right axis) when V_G was applied in the M1-phase. (b) I_G (left axis) and R (right axis) as function of V_G show the modulation in rutile phase. (c) $R-T$ plots at $V_G = 0$ before and after sweeps. The suppression of MIT even at $V_G = 0$ after gate sweep measurement is a signature of permanent chemical change. (d) Schematic of the selective electrochemical reactivity towards oxygen vacancies formation.

Fig. 4 (a) compares the electrochemical reactivity of rutile (left axis) and monoclinic phases (right axis) of VO_2 during the electrolyte gating by taking data from Fig. 2 (a) and Fig. 3 (a). It can be seen that even $V_G = 1.2$ V applied in the rutile phase is sufficient to stabilize the metallic phase down to room temperature. However, V_G applied in the monoclinic phase fails to stabilize the metallic phase and the device exhibits insulating behavior ($R = 5.5 \times 10^5$ Ω at 310 K to 1950 Ω at 335 K) even at a bias of 2.5 V in the temperature range.

In order to further understand the temperature dependent modulations and redox kinetics, gate sweep measurements were done in rutile phase at 380 K. The device resistance can be modulated by gating in the metallic phase as can be seen in the plots of the evolution of I_G (left axis) and R (right axis) with V_G at 380 K (Fig. 4 (b)). The device resistance was found to be increasing with the increase in V_G similar to Fig. 2 (a) where the resistance of

the metallic phase increases with V_G. Asymmetric peaks were once again observed in the $I_G - V_G$ plot. However, the $I_G - V_G$ plot at 380 K has larger peaks with less separation between the peaks at positive and negative gate biases suggesting faster electrode reactions, likely facilitated by faster charge transfer at the now more conducting VO_2 electrode. The current peaks i_{pa} and i_{pc} arise from the oxidation and reduction processes respectively from gate/IL/VO_2 system. In the case of a reversible redox reaction, the peaks are related as $E_{pa} - E_{pc} = 0.059V/n$, where E_{pa} and E_{pc} are the oxidation and reduction peak positions and n is the number of electrons transferred across the IL/electrode interface[23–25]. Fig. 4 (b) shows that i_{pa} and i_{pc} are asymmetric at E_{pa} and E_{pc} respectively and $E_{pa} - E_{pc} > 0.059V$ pointing to the irreversible nature of the redox reactions at the interface.

Fig. 4 (c) shows $R-T$ plots measured at $V_G = 0$ before and after the gate sweeps shown in Fig. 4 (b). In contrast to the V_G sweeps in the monoclinic phase, the V_G sweeps in the rutile phase at 380 K irreversibly change the electronic properties of the nanobeam. It can be seen that the V_G sweeps (Fig. 3 (a)) modulate the resistance reversibly at temperatures of 310 K, 315 K, and 320 K, whereas similar V_G sweeps at 380 K (Fig. 4 (b)) suppresses the MIT completely (Fig. 4 (c)) indicating an irreversible chemical transformation. Based on these observations, we can infer that the kinetics of the electrochemistry involved for the creation of oxygen vacancies strongly depends on the structural phase and temperature as shown by the schematic in the Fig. 4 (d). Similar selective behavior has been observed in the case of hydrogen doping[27,28] in VO_2 and the diffusion constant for hydrogen was found to be orders of magnitude higher in the rutile phase than in the monoclinic phase[27,28]. Though previous studies of IL gating in oxide materials have shown the suppression of MIT and discussed the role of oxygen vacancies[7,15], we show, for the first time, that the application of a gate bias in the rutile phase is crucial for stabilizing it even to lower temperatures.

A control gating measurement was done on a device with same structure as in the inset of Fig. 1 (b) but without the VO_2 nanobeam in order to delineate the role of gold electrodes in the electrochemical reaction and their contribution to I_G. If I_G is purely electrostatic in origin, the magnitude of I_G should be similar for devices with and without the nanobeam since the area of the VO_2 nanobeam is negligible compared to the area of electrodes under the IL drop. The absence of any peak like features in Fig. 5 (a), (b), (c) shows that I_G in this case is mostly electrostatic in nature. Moreover, I_G at 2.2 V is smaller by $\sim$ 15 times at 300 K, $\sim$ 6 times at 330 K and 380 K when compared to I_G of an identical

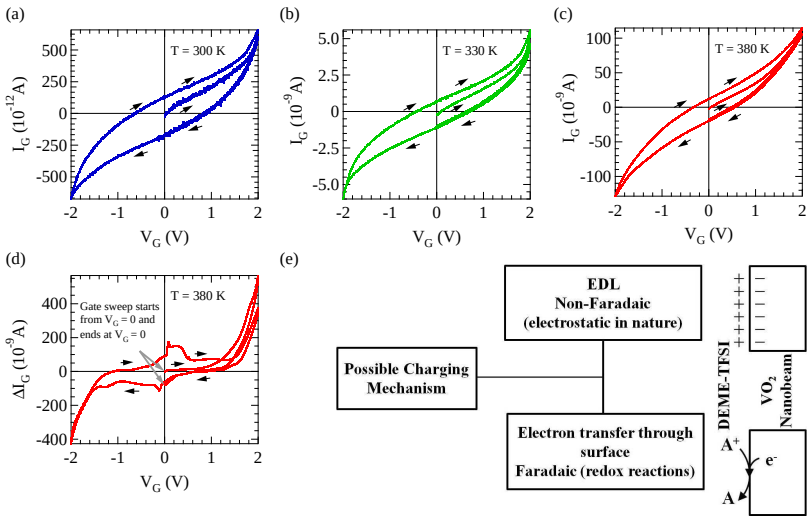

FIG. 5. (a), (b), and (c) show gate sweep measurements of a device with a similar S-D-G arrangement as in inset of Fig. 3 (b), but without the VO_2 nanobeam (T= 300 K, 330 K and 380 K respectively). (d) Differential gate current (ΔI_G) from the IL/VO_2 interface after the contribution from the contacts is subtracted. (e) Possible charging mechanisms outlined.

device with a VO_2 nanobeam (Fig. 3 (b) and Fig. 4 (b)). This indicates that I_G for a VO_2 device has contribution due to redox reaction at the IL/VO_2 interface since the I_G-V_G plots have redox peaks. The ΔI_G (Fig. 5 (d)) was obtained by subtracting gate currents during the IL gating in devices with and without the nanobeam, where ΔI_G is only due to the electrochemical reaction at the IL/VO_2 interface. Fig. 5 (e) shows possible charging mechanisms that can be faradaic or non-faradaic and are applicable in the case of the IL gating of VO_2. The formation of an electrical double layer (EDL) at the IL/VO_2 interface is due to the migration of ions towards the electrodes in response to an electric field. The EDL formation is electrostatic in nature with no chemical change occurring either in the electrodes or in the electrolyte. However, redox reactions can oxidize/reduce an ion or an analyte (DEME-TFSI) present in the electrolyte/electrode as shown in Fig. 5(e) where an analyte A^+ will be reduced to A at the IL/VO_2 interface by accepting an electron from the VO_2 nanobeam acting as the cathode. This process will chemically change the properties of the interface involved and may lead to the misinterpretation of the resistance modulation to be electrostatic in nature. The exact redox reactions or redox couples involved during the gating processes giving rise to the oxygen vacancies are unknown. However, it might

be possible that one of the analytes present in the IL will chemisorb on the VO_2 surface to consume the lattice oxygen and when it desorbs, it will leave oxygen vacancies that can be either filled by oxygen atoms in the VO_2 bulk or by the gaseous oxygen present in the chamber[29]. The redox reaction might also be mediated by the Au/VO_2 interface as the metal/metal-oxide interface is known to be very reactive for oxygen evolution. For instance, oxygen vacancies are much more easily created in CeO_2 in the presence of Au[30]. Previous studies have shown the reduction of the vanadium oxidation state from V^{4+} towards V^{3+} due to the introduction of oxygen vacancies[7,17]. It is important to note that the ionic radius of V^{3+} is larger than V^{4+} and therefore expansion in lattice parameter is expected and it will lead to strain within the nanobeam. A recent study on VO_2 reported a strong deformation in lattice structure during the IL gating process[11,18].

IV. RAMAN SPECTROSCOPY MEASUREMENTS

To elucidate the structural changes during the ionic liquid gating process, we performed Raman spectroscopy measurements at 300 K on our devices before and after gating and the results are presented in Fig. 6. The spectra were taken from VO_2 single nanobeam devices and from a VO_2 film prepared by electrophoretic deposition of the nanobeams. In Fig. 6 (a), Raman spectra acquired at 300 K from a VO_2 nanobeam device immediately after application of a gate voltage are shown; the pristine device (top trace) shows the characteristic Raman bands of the monoclinic (M1) phase of VO_2[22]. After application of a positive gate voltage of +1.8 V, the resistance of the device at 300 K is reduced by more than three orders of magnitude; however, a complete suppression of the MIT was not yet achieved (see Fig. 2 (a)). The device was washed with isopropyl alcohol, deionized water and blow dried to remove any remnant electrolyte on the surface. The gating induced resistance modulations were unaffected for a few days and Raman spectra were taken in this intermediate state. Spectra acquired from two different locations (Fig. 6 (a)) show that the characteristic Raman modes of the monoclinic M1 phase are diminished intensity but the peak positions are not substantially shifted. This reduction in intensity of the monoclinic Raman peaks during the gating process is also verified by the Raman spectra taken acquired from a thin film of VO_2 (Fig. 6 (b)).

The spectra of gated devices show clearly that the Raman modes of the monoclinic

phase are still intact albeit with reduced intensities even after the resistance of the device is reduced by three orders of magnitude. Notably, upon transformation of VO_2 to a metallic phase, the Raman cross-section is greatly diminished and the laser skin depth is also greatly reduced by the much higher carrier density[22]. The electrochemical reactions induced by the electrolyte gating likely occur on the surface of VO_2 leading to surface metallization whereas the sub-surface layers are not metallized and contribute to the M1 peaks in the traces above[31]. Further gating to +2.2 V (bottom trace in Fig. 2 (a)) suppresses the MIT completely and the characteristic M1 peaks vanish[22]. Whereas, the Raman results are consistent with initial phase coexistence of insulating monoclinic and metallic domains (the monoclinic domains contribute to the remnant Raman intensity), this method alone cannot distinguish whether the metallized phase (corresponding to the absence of a Raman signal) is the metallic rutile phase or a different metallic structure with a distorted monoclinic or triclinic symmetry. Correlating Raman and transport data, the suppression of the MIT corresponds to formation of a (surface) percolative network of the vacancy-induced metallic phases with coexistence of remnant monoclinic domains. Indeed, the steps in resistance observed in the transport data correspond to the dynamic switching of these domains. At higher gate voltages, the entire nanowire can be metallized (as per Raman measurements) and the transport behavior indicates smooth characteristics of a metal.

V. DENSITY FUNCTIONAL THEORY CALCULATIONS

We have carried out density functional theory (DFT)[32,33] based first-principles calculations using the DFT+U method[34] to understand and quantify the effects of oxygen vacancies and its formation mechanism under IL gating conditions. Note that we do not attempt to address other possible IL-VO_2 interfacial effects here. All calculations presented in the manuscript were performed using the Quantum Espresso package[35]. The Perdew-Burke-Ernzerhof (PBE) functional within the generalized gradient approximation (GGA) is used[36]. A moderate screened on-site Coulomb energy (U) of 3.0 eV is applied to vanadium d electrons. This value is consistent with that calculated from a constrained random phase approximation approach[37], and gives a band gap of 0.67 eV for the M1 phase. Electron-ion interactions are described by ultrasoft pseudopotentials[38] and a 40 Ry energy cutoff is used for the plane wave expansion of the wave functions. Fig. 7 (a) compares the density of states

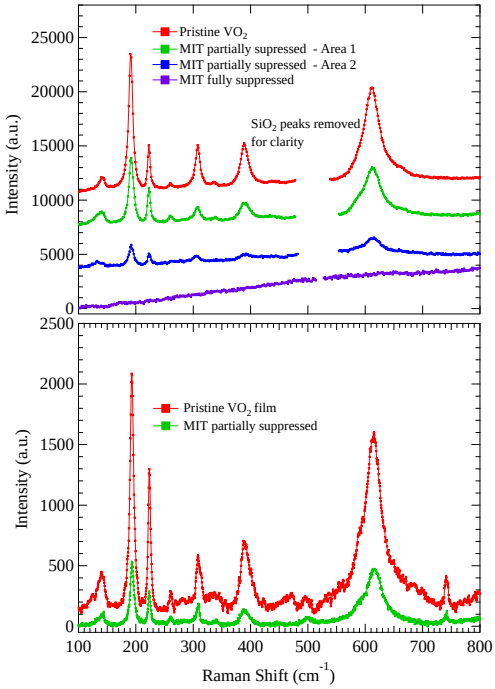

FIG. 6. (a) Comparison of Raman spectra acquired at 300 K for a VO_2 nanobeam device during the gating process. The traces are offset for clarity. The Raman bands of the pristine VO_2 device undergo a drastic reduction in intensity during the gating process as seen by the top three traces; however, the characteristic Raman modes of the monoclinic M1 phase are still retained suggesting the initiation of metallization on the surface. In a device where the MIT is fully suppressed (similar to the +2.2 V trace in Figure 2), the absence of discernible Raman modes can be attributed to metallization, likely originating from stabilization of the metallic phase. (b) Raman spectra taken from a VO_2 nanobeam film before and after partial gating corroborating the results from a single nanowire device. The diminution of the Raman intensities can be attributed to surface metallization with remnant domains of the M1 phase contributing to the observed signal.

(DOS) for the ideal VO_2 (M1 phase) and VO_2 with an oxygen vacancy (1 oxygen vacancy in a 144-atom cell). The ideal system shows a band gap of $\sim$ 0.67 eV from the DFT+U method. To better compare the DOS of the ideal and defective system, we have done the following. First, the valence band maximum (VBM) of the ideal system is shifted to zero in the plot. Second, the chemical potential of the defective system is measured from the VBM of the ideal system. With the presence of an oxygen vacancy (in a 144-atom cell), the $a_{1g}(d_{x^2-y^2})$ valence states are significantly affected. In addition, oxygen vacancies introduce

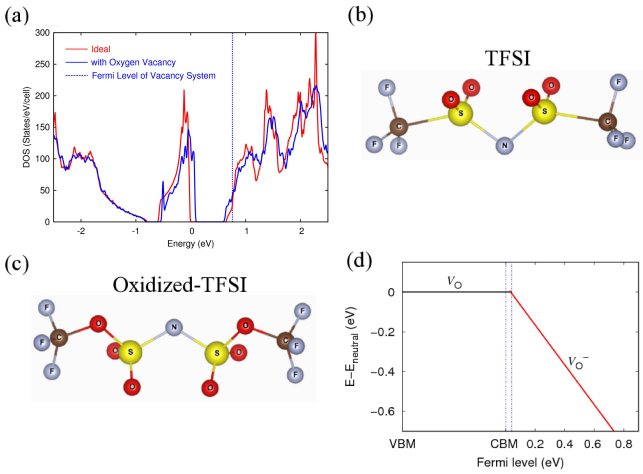

FIG. 7. (a) Density of states (DOS) of VO_2 with (blue) and without (red) oxygen vacancy showing enhanced DOS in the energy gap. The vertical dashed line shows the Fermi level of the vacancy system. (b) TFSI molecule. (c) Oxidized TFSI. (d) Calculated relative formation energy as a function of the Fermi level for neutral (V_O) and negatively charged (V_{O-}) state.

defect (donor) states which merge with the conduction band edge, suggesting the possibility of an oxygen-vacancy induced modification of the MIT. Oxygen vacancies also results in a significant local rearrangement of V-V bonding network, which further destabilizes the insulating phase. In the ideal VO_2 M1 phase, vanadium atoms form alternating long and short bonds with bond lengths of 2.5 and 3.2 Å. The presence of oxygen vacancies significantly disturbs the V-V dimerization resulting in intermediate bond lengths. The formation of these intermediate bond lengths also results in a substantial electron delocalization along the V-chains as compared to the ideal case. It is widely accepted that the V-V dimerization is critical for the stability of the insulating M1 phase, and the weakening of the V-V dimerization by oxygen vacancies would naturally result in a lower phase transition temperature as can be seen in Fig. 2 (a)[39].

One important question that remains to be answered is how the IL gating could result in the generation of oxygen vacancies. To this end, we have carried out first-principles calculations to characterize the energetics of oxygen vacancy formation. We find that with the application of a gating voltage, it is thermodynamically favorable to form oxygen vacancies in VO_2 if the TFSI molecules (Fig. 7 (b)) are oxidized by oxygen atoms released from VO_2 as shown in Fig. 7 (c). First, we assume that both TFSI and VO_2 are charge neutral. The

formation of one oxygen vacancy in VO_2, with the oxidized TFSI molecule (Fig. 7 (c)), is 0.51 eV per vacancy in the rutile phase as compared to 1.41 eV in the monoclinic phase. This result is in consistent with our conclusion based on the experimental finding in Figures 2, 3, and 4 that oxygen vacancies creation is more favorable in the rutile phase. In addition, even for the monoclinic phase, the chemical potential of the VO_2 can be tuned by V_G in order to generate negatively charged oxygen vacancies to further lower the defect formation energy. Fig. 7 (d) shows the relative formation energy of a neutral and a negatively charged oxygen vacancy. The upward shift of the chemical potential can significantly lower the formation energy of a negatively charged oxygen vacancy and results in vacancy generation becoming thermodynamically favorable.

VI. CONCLUSIONS

In conclusion, we find that the electrolyte gating induced resistance modulation in single-crystalline VO_2 nanobeams is electrochemical in origin. Our results show that the electrochemical reactivity during electrolyte gating measurements is greatly enhanced in the rutile (metallic) phase as compared to the monoclinic (insulating) phase. Our density functional theory (DFT) calculations show that this accommodation of high concentration of oxygen vacancies in the rutile phase results in disturbing the V-V dimerization and can lead to the stabilization of the rutile phase to lower temperatures and can explain the complete suppression of the metal-insulator transition. The generation of oxygen vacancies is thermodynamically favored if the removed oxygen atoms from VO_2 oxidize the TFSI anions. Raman spectroscopy data suggest surface metallization upon electrolyte gating with initial coexistence of insulating monoclinic and metallic domains.The selective electrochemical reactivity of the rutile phase in VO_2 and the resulting defect-induced stabilization of this phase across a vastly expanded temperature window suggests a facile defect engineering route to tune electronic phase transitions in several correlated electron oxide systems as active channel in an electrolyte-gated FET.

ACKNOWLEDGMENTS

This work was supported by the National Science Foundation under DMR 0847324; PZ acknowledges supports from the National Science Foundation under Grant DMR 0946404 and DMR 1506669, and the SUNY Networks of Excellence and computational support provided by the Center for Computational Research at the University at Buffalo; G. A. H, P. M, and S.B. acknowledge support from the National Science Foundation under IIP 1311837. Correspondence and requests for materials should be addressed to G. S.

---

* sg82@buffalo.edu

[1] M. K. Nowotny, L. R. Sheppard, T. Bak, and J. Nowotny, J. Phys. Chem. C **112**, 5275 (2008).

[2] J. B. Yi, C. C. Lim, G. Z. Xing, H. M. Fan, L. H. Van, S. L. Huang, K. S. Yang, X. L. Huang, X. B. Qin, B. Y. Wang, T. Wu, L. Wang, H. T. Zhang, X. Y. Gao, T. Liu, A. T. S. Wee, Y. P. Feng, and J. Ding, Phys. Rev. Lett. **104**, 137201 (2010).

[3] Y. Li, R. Deng, B. Yao, G. Xing, D. Wang, and T. Wu, Appl. Phys. Lett. **97**, 102506 (2010).

[4] N. J. Lawrence, J. R. Brewer, L. Wang, T.-S. Wu, J. Wells-Kingsbury, M. M. Ihrig, G. Wang, Y.-L. Soo, W.-N. Mei, and C. L. Cheung, Nano Lett. **11**, 2666 (2011).

[5] U. Aschauer, R. Pfenninger, S. M. Selbach, T. Grande, and N. A. Spaldin, Phys. Rev. B **88**, 054111 (2013).

[6] F. J. Morin, Phys. Rev. Lett. **3**, 34 (1959).

[7] J. Jeong, N. Aetukuri, T. Graf, T. D. Schladt, M. G. Samant, and S. S. P. Parkin, Science **339**, 1402 (2013).

[8] Z. Yang, Y. Zhou, and S. Ramanathan, J. Appl. Phys. **111**, 014506 (2012).

[9] M. Nakano, K. Shibuya, D. Okuyama, T. Hatano, S. Ono, M. Kawasaki, Y. Iwasa, and Y. Tokura, Nature **487**, 459 (2012).

[10] J. S. Sim, Y. Zhou, and S. Ramanathan, Nanoscale **4**, 7056 (2012).

[11] D. Okuyama, M. Nakano, S. Takeshita, H. Ohsumi, S. Tardif, K. Shibuya, T. Hatano, H. Yumoto, T. Koyama, H. Ohashi, M. Takata, M. Kawasaki, T. Arima, Y. Tokura, and Y. Iwasa, Appl. Phys. Lett. **104**, 023507 (2014).

[12] K. Ueno, H. Shimotani, Y. Iwasa, and M. Kawasaki, Appl. Phys. Lett. **96**, 252107 (2010).

[13] S. Asanuma, P.-H. Xiang, H. Yamada, H. Sato, I. H. Inoue, H. Akoh, A. Sawa, K. Ueno, H. Shimotani, H. Yuan, M. Kawasaki, and Y. Iwasa, Appl. Phys. Lett. **97**, 142110 (2010).

[14] H. Ji, J. Wei, and D. Natelson, Nano Lett. **12**, 2988 (2012).

[15] M. Y. Li, W. Han, X. Jiang, J. Jeong, M. G. Samant, and S. S. P. Parkin, Nano Lett. **13**, 4675 (2013).

[16] T. D. Schladt, T. Graf, N. B. Aetukuri, M. Li, A. Fantini, X. Jiang, M. G. Samant, and S. S. P. Parkin, ACS Nano **7**, 8074 (2013).

[17] J. Karel, C. E. ViolBarbosa, J. Kiss, J. Jeong, N. Aetukuri, M. G. Samant, X. Kozina, E. Ikenaga, G. H. Fecher, C. Felser, and S. S. P. Parkin, ACS Nano **8**, 5784 (2014).

[18] J. Jeong, N. B. Aetukuri, D. Passarello, S. D. Conradson, M. G. Samant, and S. S. P. Parkin, Proc. Natl. Acad. Sci. U.S.A. **112**, 1013 (2015).

[19] Y. Zhou, J. Park, J. Shi, M. Chhowalla, H. Park, D. A. Weitz, and S. Ramanathan, Nano Lett. **15**, 1627 (2015).

[20] B. J. Morgan and G. W. Watson, J. Phys. Chem. C **113**, 7322 (2009).

[21] Z. Wu, M. Li, and S. H. Overbury, J. Catal. **285**, 61 (2012).

[22] G. A. Horrocks, S. Singh, M. F. Likely, G. Sambandamurthy, and S. Banerjee, ACS Appl. Mater. Interfaces **6**, 15726 (2014).

[23] R. S. Nicholson and I. Shain, Anal. Chem. **36**, 706 (1964).

[24] R. S. Nicholson, Anal. Chem. **37**, 1351 (1965).

[25] J. Heinze, Angew. Chem. Int. Ed. Engl. **23**, 831 (1984).

[26] Y. Zhou and S. Ramanathan, J. Appl. Phys. **111**, 084508 (2012).

[27] J. Wei, H. Ji, W. Guo, A. H. Nevidomskyy, and D. Natelson, Nat. Nanotechnol. **7**, 357 (2012).

[28] J. Lin, H. Ji, M. W. Swift, W. J. Hardy, Z. Peng, X. Fan, A. H. Nevidomskyy, J. M. Tour, and D. Natelson, Nano Lett. **14**, 5445 (2014).

[29] P. Mars and D. W. van Krevelen, Chem. Eng. Sci. **3**, 41 (1954).

[30] Y. Lee, G. He, A. J. Akey, R. Si, M. Flytzani-Stephanopoulos, and I. P. Herman, J. Am. Chem. Soc. **133**, 12952 (2011).

[31] Y. Zhou, J. Park, J. Shi, M. Chhowalla, H. Park, D. A. Weitz, and S. Ramanathan, Nano Letters **15**, 1627 (2015).

[32] P. Hohenberg and W. Kohn, Phys. Rev. **136**, B864 (1964).

[33] W. Kohn and L. J. Sham, Phys. Rev. **140**, A1133 (1965).

[34] V. I. Anisimov, J. Zaanen, and O. K. Andersen, Phys. Rev. B **44**, 943 (1991).

[35] P. Giannozzi, S. Baroni, N. Bonini, M. Calandra, R. Car, C. Cavazzoni, D. Ceresoli, G. L. Chiarotti, M. Cococcioni, I. Dabo, A. Dal Corso, S. de Gironcoli, S. Fabris, G. Fratesi, R. Gebauer, U. Gerstmann, C. Gougoussis, A. Kokalj, M. Lazzeri, L. Martin-Samos, N. Marzari, F. Mauri, R. Mazzarello, S. Paolini, A. Pasquarello, L. Paulatto, C. Sbraccia, S. Scandolo, G. Sclauzero, A. P. Seitsonen, A. Smogunov, P. Umari, and R. M. Wentzcovitch, J. Phys.: Condens. Matter **21**, 395502 (2009).

[36] J. P. Perdew, K. Burke, and M. Ernzerhof, Phys. Rev. Lett. **77**, 3865 (1996).

[37] B.-C. Shih, T. A. Abtew, X. Yuan, W. Zhang, and P. Zhang, Phys. Rev. B **86**, 165124 (2012).

[38] D. Vanderbilt, Phys. Rev. B **41**, 7892 (1990).

[39] X. Yuan, W. Zhang, and P. Zhang, Phys. Rev. B **88**, 035119 (2013).